Causes and health risk assessment of fluorine in the Red bed groundwater and adjacent geothermal water of the Guang'an Area, Southwest China

Yu-xiang Shao[1], Wei Zhang[1,2*], Wen-bin Chen[1*], Li Chen[1], Jian Li[1], Guang-long Tian[1], Li-cheng Quan[1], Bu-qing Yan[1,3], Yu-jie Liu[2]

[1] *Research Center of Applied Geology of China Geological Survey, Chengdu 610000, China.*
[2] *School of Water Resources and Environment, China University of Geosciences (Beijing), Beijing 100083, China.*
[3] *School of Earth Sciences, China University of Geosciences (Wuhan), Wuhan 430074, China.*

Abstract: Understanding the levels, causes, and sources of fluoride in groundwater is critical for public health, effective water resource management, and sustainable utilization. This study employs multivariate statistical methods, hazard quotient assessment, and geochemical analyses, such as mineral saturation index, ionic activities, and Gibbs diagrams, to investigate the hydrochemical characteristics, causes, and noncarcinogenic risks of fluoride in Red bed groundwater and geothermal water in the Guang'an area and neighboring regions. Approximately 9% of the Red bed groundwater samples contain fluoride concentrations exceeding 1 mg·L^{-1}. The predominant water types identified are Cl-Na and HCO$_3$-Na, primarily influenced by evapotranspiration. Low-fluoride groundwater and high-fluoride geothermal water exhibit distinct hydrochemical types HCO$_3$-Ca and SO$_4$-Ca, respectively, which are mainly related to the weathering of carbonate, sulfate, and fluorite-containing rocks. Correlation analysis reveals that fluoride content in Red bed groundwater is positively associated with Na$^+$, Cl$^-$, SO$_4^{2-}$, and TDS (r^2 = 0.45–0.64, p < 0.01), while in geothermal water, it correlates strongly with pH, K$^+$, Ca^{2+}, and Mg^{2+} (r^2 = 0.52–0.80, p < 0.05). Mineral saturation indices and ionic activities indicate that ion exchange processes and the dissolution of minerals such as carbonatite and fluorite are important sources of fluoride in groundwater. The enrichment of fluorine in the Red bed groundwater is linked to evaporation, cation exchange and dissolution of fluorite, caused by the lithologic characteristics of the red bed in this area. However, it exhibits minimal correlation with the geothermal water in the adjacent area. The noncarcinogenic health risk assessment indicates that 7% (n = 5) of Red bed groundwater points exceed the fluoride safety limit for adults, while 12% (n = 8) exceed the limit for children. These findings underscore the importance of avoiding highly fluoridated red bed groundwater as a direct drinking source and enhancing groundwater monitoring to mitigate health risks associated with elevated fluoride levels.

Keywords: Guang'an area; Red bed groundwater; Geothermal water; Fluoride contamination; Causes; Health risk assessment

Received: 28 Apr 2024/ Accepted: 21 Mar 2025/ Published: 10 May 2025

Introduction

Fluoride is an essential trace element for the

human body, contributing to the prevention of tooth decay and the improvement of bone health (Khatri and Tyagi, 2015; Liu et al. 2021; Liu et al. 2024). However, prolonged exposure to high levels of fluoride in drinking water can lead to fluorosis, manifesting in symptoms such as dental fluorosis, nausea, abdominal pain, and arthritis (Zhang et al. 2023). Numerous studies have highlighted that endemic fluorosis is a significant global health issue, affecting an estimated 200 million people in regions where shallow or deep groundwater is frequently extracted for drinking and daily use (Podgorski and Berg, 2022). In China, the Stan-

dard for Groundwater Quality (GB/T 14848–2017) specifies a desirable maximum fluoride concentration of 1.0 mg·L^{-1} in drinking water. Groundwater with fluoride levels exceeding this threshold is classified as high-fluorine groundwater, posing potential health risks to the affected populations.

Fluorine-containing waste from human activities, such as coal mining, agricultural fertilization, and atmospheric deposition, can contribute significantly to groundwater fluoride levels through leaching and infiltration (Zhang et al. 2021). Additionally, the formation of naturally occurring high-fluoride water is often more extensive, with complex underlying mechanisms (Gao et al. 2014; Hao et al. 2018). For example, acidic volcanic rocks and hydrothermal deposits rich in fluorine-bearing minerals can readily lead to fluoride enrichment in aquifers (Kumar et al. 2020; Podgorski and Berg, 2022). Moreover, cation exchange in groundwater can result in a high Na/Ca ratio, which promotes the dissolution of CaF_2 (Chae et al. 2007; Wen et al. 2013). Similarly, weakly alkaline or alkaline water-rock interaction facilitate the desorption of fluoride from oxides or clays (Feng et al. 2020). These findings indicate that mineral dissolution, cation exchange, and desorption are the primary processes controlling the entry of fluorine into groundwater. High-fluoride groundwater is commonly found in coastal regions, geothermal areas, arid or semi-arid zones, as well as in inland basins and plains (Durrani and Farooqi, 2021; Xing et al. 2023; Zhou et al. 2016). In coastal zones, seawater intrusion increases Na$^+$ and decreases Ca^{2+}, enhancing fluorite dissolution (Zhang et al. 2024). Geothermal water, which often contains elevated fluoride concentrations, can migrate into adjacent aquifers, contributing to fluoride contamination (Ali et al. 2016; Li et al. 2020). In regions with hot climates or slow groundwater flow, evaporation can lead to Cl-Na and HCO$_3$-Na type water bodies, further exacerbating fluoride dissolution and concentration (He et al. 2020; Jia et al. 2019). Collectively, factors such as dry climatic conditions, flat terrain that hinders groundwater runoff, seawater intrusion, evaporation, and geothermal water mixing are key factors in driving the natural enrichment of fluoride in groundwater.

Red beds refer to red terrestrial clastic rocks formed in dry and hot environments during the Mesozoic era. These formations are widely distributed across South China, Southwest China, and Central and Western China (Sheldon, 2005). Reports indicate that groundwater in the flat terrains of Red bed regions, such as Ganzhou, exhibits characteristics of fluorine enrichment

(Luo, 2020). The Guang'an area, located on the eastern margin of the Sichuan Basin in South China, faces a shortage of groundwater resources (Dong et al. 2021; Zhang et al. 2018). This region is characterized by the widespread development of near-horizontal Red beds and the presence of abundant high-fluorine geothermal water resources in the eastern parallel valley area (Chen et al. 2020; Li et al. 2020; Xiao et al. 2011). These factors may have contributed to the enrichment of fluoride in the local groundwater. Given the limited research on the characteristics of fluorine in Red bed groundwater, this study focuses on the Guang'an area, where extensive Red bed formations are present. The objectives of this study are: (i) Explore the characteristics and causes of fluoride content in the Red bed groundwater and adjacent geothermal water in the Guang'an area; (ii) Analyze the relationship between fluorine content in red bed groundwater and high-fluoride geothermal water in neighboring parallel valleys; and (iii) Evaluate the noncarcinogenic health risk associated with fluoride in groundwater. This study aims to provide fundamental data to support the safe utilization and management of local groundwater resources.

1 Study area

1.1 Geographical position and geology

The Guang'an area is located in the eastern Sichuan Province, near Chongqing to the southeast. Geographically, the region lies between 30°00′N–30°50′N and 106°00′E–107°20′E. The west-central part of Guang'an is characterized by hilly and gently sloping terrain, with elevations ranging from 180 m to 500 m. In contrast, the eastern region features low mountainous landscapes with parallel canyons, including the Huaying Mountains, the Tongluo Mountains, and the Mingyue Mountains, with elevations ranging from 600 m to 1,700 m.

Surface runoff is prevalent in the study area (Xie et al. 1981). The ridgeline of the Huaying Mountains serves as a natural divide between the Yulin River watershed to the east and the Jialing River watershed to the west. The Qujiang River, a significant tributary of the Jialing River, flows from north to south through the central region. The Dahong River, a major tributary of the Yulin River, is located between the Tongluo Mountains and the Mingyue Mountains (Figs. 1a and 1b).

The study area experiences a warm and humid subtropical monsoon climate, characterized by

abundant heat and rainfall. The average annual precipitation ranges from 1,000 mm to 1,500 mm, while the mean temperature records approximately 17.6°C (Lei and Liu, 2022).

The tectonic history of the region is complex, influenced by the large-scale southeast to northwest retrograde thrusting within the South China Plate during the Yanshan period (Xie et al. 1981). These tectonic processes have shaped the strata in the eastern parallel canyons into belt-like formations. The geology of this area primarily consists of Triassic, Permian, and Silurian strata, which include carbonate rocks, mudstones, sandstones, gypsolyte rocks, coal seams, and basalts (Fig. 1c). In contrast, the stratigraphy of the west-central part is dominated by subhorizontal Jurassic terrestrial sedimentary strata, predominantly composed of sandstones, siltstones, mudstones, and shales, collectively referred to as the Red beds. Quaternary sedi-

ments in the Red bed areas are relatively shallow and are more prominently developed on river and lake terraces (Chen et al. 2020; Sheldon, 2005).

1.2 Hydrogeology

The investigated region is a relatively open hilly area where groundwater primarily flows from east to west, influenced by the topography, stratigraphy, and tectonic features (Xie et al. 1981). The area is broadly divided into two hydrogeological segments: The complex hydrogeological zone in the eastern fold belt and the straightforward hydrogeological zone in the central-western region (Xie et al. 1981). In the complex hydrogeological zone, groundwater is mainly composed of clastic pore water, clastic fissure water, and karst water, typically exhibiting pressurized characteristics (Fig. 2). The geothermal gradient in the folded fold belt
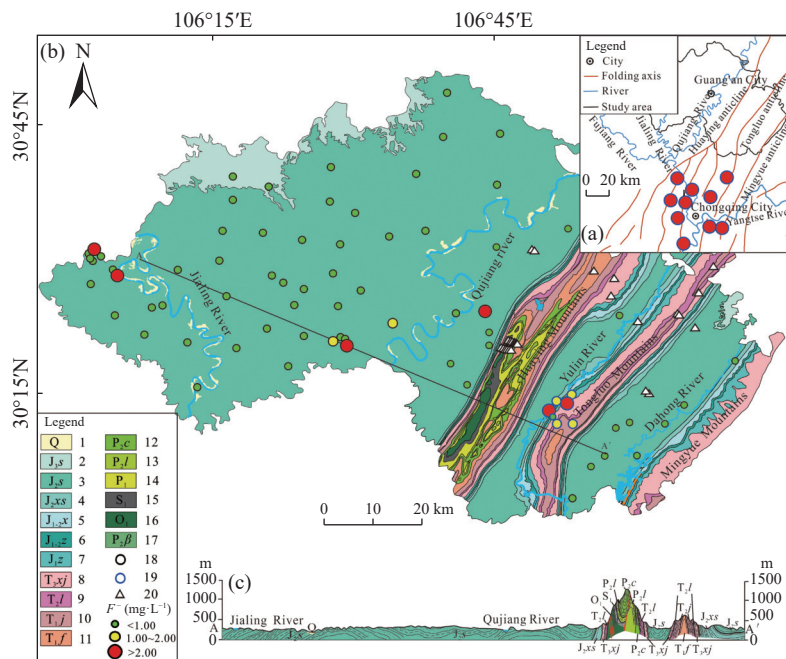

Fig. 1 (a) Map of Guang'an area; (b) Regional geology, distribution of sampling points and spatial distribution of fluoride in groundwater within the study area; (c) Typical geological profile in the study area

Notes: This figure was modified from the regional geological map released by the GeoCloud Platform of the China Geological Survey and the Guang'an Hydrogeological Report by Xie et al. (1981).

1. Quaternary: Clay and gravel; 2. Suining Fm (Formation): Mudstone with sandstone, containing thin layers of gypsum; 3. Upper Shaximiao Fm: Mudstone with sandstone, containing thin layers of carbonate and gypsum; 4. Lower Shaximiao Fm: Variegated mudstone and shale with sandstone, small amounts of limestone, containing carbonate and fluorite; 5. Xintiangou Fm: Variegated mudstone and shale with limestone, containing carbonate and fluorite; 6. Ziliujing Fm: Variegated mudstone and shale with limestone, containing carbonate and fluorite; 7. Zhenzhuchong Fm: Mudstone and shale with limestone, containing carbonate and fluorite; 8. Xujiahe Fm: Sandstone with shale and thin coal seams, containing sulfide, sulfate, and carbonate; 9. Leikoupo Fm: Dolomite interspersed with shale, containing halite, sylvite, carbonate, and fluorite; 10. Jialingjiang Fm: Dolomite interspersed with shale, containing halite, sylvite, carbonate, and fluorite; 11. Feixianguan Fm: Argillaceous limestone with shale and coal seams, containing carbonate, sulfide, halite, sulfate, and fluorite; 12. Changxing Fm: Argillaceous limestone with shale, containing halite, carbonate, and fluorite; 13. Longtan Fm: Argillaceous limestone with shale, containing halite, carbonate, and fluorite; 14. Lower Permian Series: Mudstone and shales; 15. Lower Silurian Serie: Mudstone and shales; 16. Lower Ordovician Series: Dolomite and siliceous limestone; 17. Emei Mountain basalt; 18. Red bed groundwater samples of this study; 19. Geothermal water (Li et al. 2020; Xiao et al. 2011); 20. Rock samples.

region, along with the inclined and fissured gypsolyte rock layers, create favorable conditions for the formation of geothermal water (Li et al. 2020; Qian et al. 2012). Geothermal water circulates along the flanks of the folds, interacting with soluble minerals in the Triassic strata, including carbonate, sulfide, sulfate, fluorite, halite, and sylvite (Fig. 1). As the water descends deeper, it absorbs heat, causing its temperature to rise (Qian et al. 2012). Given the stratum's inclination and the abundance of structural fissures and caves, groundwater in this area is substantially recharged by atmospheric precipitation and rivers traversing the area. The outflow of geothermal water is particularly swayed by karst channels, tectonic fissures, and interlayer fissures. Discharge typically occurs through spring points, karst culverts, and human extractions for physiotherapy baths.

In the straightforward hydrogeological region, bedrock fissure water is the dominant groundwater type in the Red bed area, supplemented by residual Quaternary loose pore water (Xie et al. 1981). The bedrock fissure water in these areas is greatly influenced by the thickness of the weathering crust and the presence of horizontally bedded mudstone or shale, which are widely distributed across the red bed region (Xie et al. 1981). As a result, groundwater resources are relatively scarce and singular, with limited soluble minerals interacting with the groundwater, primarily consisting of carbonate, fluorite, and gypsum from the Jurassic strata in the runoff area (Fig. 1). The principal sources for this groundwater are atmospheric rainfall and surface runoff within the Red bed area. Recharge processes are predominantly affected by the undulating hilly landscape and permeable layers, such as the stratified sandstone. Groundwater in the Red bed region typically occurs at shallow depths, and its discharge is mainly facilitated by evapotranspiration and artificial pumping.

2 Materials and methods

2.1 Sample collection and measurement

Between 2022 and 2023, a total of 68 groundwater samples and 27 rock samples were collected from the red beds within the Guang'an area (Fig. 1). The groundwater samples were collected from civilian wells, situated away from pollution sources such as farms and landfills, and primarily consisted of red bed pore water, with depths not exceeding 50 m. pH levels were measured in situ using a portable multiparameter water analysis device (Manta, Eureka, Inc., Austin, TX, USA), which has a calibration accuracy of ±0.05. During collection, clean polyethylene bottles were rinsed three times with the sampling water. The samples were generally collected below 0.2 m of the water surface and filtered through a 0.45-micron cellulose acetate membrane. The filtered samples were stored in 500 mL collection containers and transported to the laboratory in a holding tank at a low temperature of 4°C.

All sample tests were conducted at the Chengdu Analytical and Testing Center in Sichuan Province, China. Parallel samples were used to ensure the accuracy of the tests. Total Dissolved Solids (TDS) were measured using an electrothermal constant temperature drying oven at 180°C, and the samples
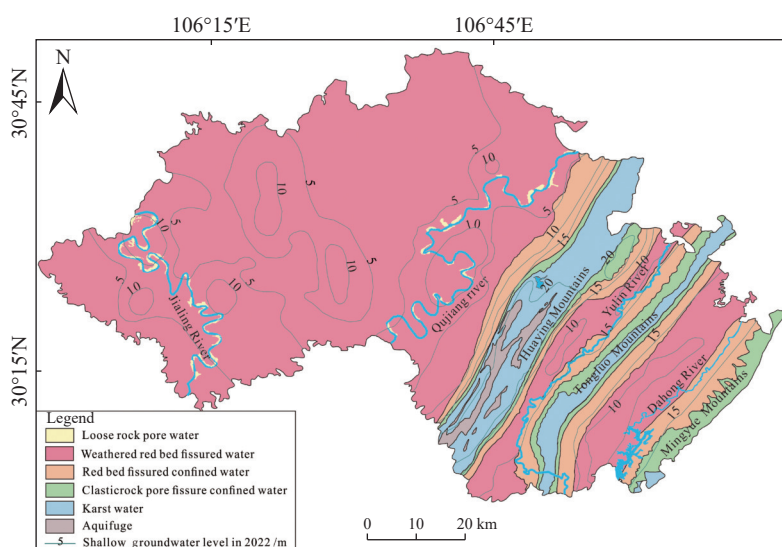

Fig. 2 Schematic map of hydrogeology and shallow groundwater level of the study area

were weighed with an analytical balance, which had an accuracy of ±0.2%. Alkalinity was quantified through a titration technique using phenolphthalein as the benchmark, with an accuracy of 0.05 mg·L⁻¹. The concentrations of Na^+, K^+, Ca^{2+}, and Mg^{2+} were analyzed using inductively coupled plasma atomic emission spectrometry (ICAP6000, Thermo Fisher Scientific, Inc., USA), with detection limits of 0.01 mg·L⁻¹. The concentrations of Cl^-, SO_4^{2-}, and F^- were measured using ion chromatography (ICS2000, Thermo Fisher Scientific, Inc., USA), with detection limits of 0.01 mg·L⁻¹. The absolute error for anion and cation concentrations was assessed to ensure accuracy being less than 5%. The fluorine contents in the rock samples were determined using the selective electrode method. The tested results were compared with geothermal water samples from published sources (Li et al. 2020; Xiao et al. 2011) (Fig. 1) to identify differences in hydrochemical properties.

2.2 Health risk evaluation

The Health Risk Assessment (HRA), which integrates the recommended reference dose with daily intake through various exposure routes, effectively evaluates the potential risks to human health from ingested substances (Aghapour et al. 2018; Lan et al. 2024). Since fluorine in drinking water primarily causes noncarcinogenic effects on human health, the Hazard Quotient (*HQ*) in the HRA model was used to evaluate its noncarcinogenic risk in drinking water (USEPA, 1987; Zhang et al. 2018). The *HQ* is calculated using the following formulas:

$$HQ = ADD/RfD \tag{1}$$

$$ADD = (C \times IR \times EF \times ED)/(BW \times AT) \tag{2}$$

Where: *ADD* represents the average daily intake of fluoride from potable water. *C* is the analyzed concentration of F^- in groundwater. *IR* stands for daily intake of drinking water. *EF* refers to the exposure frequency. *ED* represents the days of exposure. *BW* represents mean weight of the target audience. The mean weights of children and adults are the recommended values for children (6–9 years old) and adults in Southwest China (Ministry

of Ecology and Environment, 2013; Ministry of Ecology and Environment, 2016). *AT* represents the average time, calculated as number of days corresponding to *ED* for noncarcinogenic effects. The reference values for each variable are summarized in Table 1. According to the United States Environmental Protection Agency, the Recommended reference Dose (*RfD*) for noncarcinogen fluorine via the dietary route is 0.06 mg·kg⁻¹·d⁻¹ (USEPA, 1987). An *HQ* greater than 1 indicates a potential noncarcinogenic hazard, while an *HQ* less than 1 suggests no potential noncarcinogenic risk for fluorine (Zhang et al. 2018).

2.3 Data processing

Microsoft Excel 2013 (Microsoft Corp., USA) was used for statistical analysis, including the average value, minimum, maximum, standard deviation, coefficient of variation, and Gibbs plots (Gibbs, 1970). Piper plots (Piper, 1944) and Pearson's correlation analyses were conducted using Origin 2021 (OriginLab, Northampton, MA, USA). ArcGIS 10.4 (Esri, Inc., Redlands, CA, USA) and CorelDRAW v18 (Corel Corp., Ottawa, CAN) were used to modify the sampling maps. The mineral saturation indices in groundwater were calculated using PHREEQC software (Kammoun et al. 2022).

3 Results

3.1 Major chemical compositions and correlation analysis in groundwater

Significant variations were observed in the chemical compositions and major properties of the red bed groundwater and geothermal water (Table 2). The pH of the Red bed groundwater ranged from 6.30 to 9.19, with an average value of 7.34, indicating a neutral to slightly alkaline condition. Total Dissolved Solid (TDS) in the Red bed groundwater varied from 148 mg·L⁻¹ to 2,520 mg·L⁻¹, with an average of 482 mg·L⁻¹. Most of the Red bed groundwater samples were classified as fresh, with only two samples exceeding the acceptable TDS limit of 1,000 mg·L⁻¹. The average concentration

Table 1 Parameters for the calculation of the HRA model in this study

Parameters	C	IR	EF	ED	BW	AT	RfD
Unit	mg·L⁻¹	L·d⁻¹	d·a⁻¹	a	kg	d	mg·kg⁻¹·d⁻¹
Adult	Measured	3	120	30	57	EF×ED	0.06
Children	Measured	1.5	30	6	26	EF×ED	0.06

Table 2 Contents of major chemical compositions and fluoride in the different types of groundwater

Sample type		pH	TDS	Na^+	K^+	Ca^{2+}	Mg^{2+}	Cl^-	SO_4^{2-}	HCO_3^-	NO_3^-	F^-	Data source
Limit		6.5–8.5	1,000	200	-	-	-	250	250	-	20	1.0	(GB/T 14848–2017)
Red beds (n=68)	Min	6.30	146	5.0	0.63	8.79	1.63	0.66	6.30	26.00	0.7	0.08	This study
	Max	9.19	2,520	635.0	50.40	220.00	45.80	1,030.00	520.00	511.00	186.0	3.76	
	Ave	7.34	482	58.0	4.60	80.97	16.38	58.58	69.47	280.35	29.3	0.58	
	SD	0.49	319	91.6	7.85	39.39	8.22	140.42	76.87	114.91	33.5	0.74	
	CV	0.07	0.66	1.6	1.71	0.49	0.50	2.40	1.11	0.41	1.14	1.27	
	% > Limit	4	3	4	-	-	-	4	3	-	46	9	
Geothermal water (n=17)	Min	6.45	448	2.4	1.88	226.00	43.90	1.35	335.00	91.53	-	0.10	(Li et al. 2020; Xiao et al. 2011)
	Max	7.69	1,512	355.0	37.30	817.00	178.00	70.89	2,114.00	317.30	-	14.71	
	Ave	7.14	808	41.6	14.91	556.86	112.87	18.45	1,429.56	188.35	-	7.62	
	SD	0.32	274	78.49	10.78	216.55	46.46	14.95	638.32	51.84	-	5.35	
	CV	0.04	0.34	1.89	0.72	0.39	0.41	0.81	0.45	0.28	-	0.70	
	% > Limit	6	18	6	-	-	-	0	100	-	-	94	-

Note: The units for ion and TDS concentrations are $mg \cdot L^{-1}$. CV is the coefficient of variation, %. pH, dimensionless.

of cations and anions were as follows: $Ca^{2+} > Na^+ > Mg^{2+} > K^+$ for cations and $HCO_3^- > Cl^- > SO_4^{2-} > NO_3^- > F^-$ for anions. The fluoride (F^-) levels in the red bed groundwater varied from 0.08 $mg \cdot L^{-1}$ to 3.76 $mg \cdot L^{-1}$, with 9% of the samples exceeding the 1.0 $mg \cdot L^{-1}$ limit set by the Standard for Groundwater Quality (GB/T 14848–2017). The high-fluoride red bed groundwater was primarily distributed along the upper reaches of the Jialing River and the middle and lower reaches of the Qiujiang River, exhibiting no distinct distribution pattern within the study area. No more than 5% of the total samples had TDS, Na^+, Cl^-, SO_4^{2-}, and pH exceeding the corresponding limits specified in the Standard for Groundwater Quality (GB/T 14848–2017). Notably, approximately 46% of the samples had NO_3^- concentration exceeding the 20 $mg \cdot L^{-1}$ limit set by the standard (GB/T 14848–2017).

The pH levels in the geothermal water ranged from 6.45 to 7.69, with a mean of 7.14. The Total Dissolved Solids (TDS) concentration in the geothermal water ranged from 448 $mg \cdot L^{-1}$ to 1,512 $mg \cdot L^{-1}$, with a mean of 808 $mg \cdot L^{-1}$, which was higher than that in the red bed groundwater. The average concentration of cations and anions in the geothermal water followed the order: $Ca^{2+} > Mg^{2+} > Na^+ > K^+$ for cations and $SO_4^{2-} > HCO_3^- > Cl^- > F^-$ for anions, which differed from the order found in the Red bed groundwater. The F^- concentration in the geothermal water ranged from 0.10 $mg \cdot L^{-1}$ to 14.71 $mg \cdot L^{-1}$, with 94% of the samples exceeding the 1.0 $mg \cdot L^{-1}$ limit. The average values of SO_4^{2-}, Ca^{2+} Mg^{2+}, and K^+ in geothermal samples were 1,429.56 $mg \cdot L^{-1}$, 556.86 $mg \cdot L^{-1}$, 112.87 $mg \cdot L^{-1}$, and 14.91 $mg \cdot L^{-1}$, respectively, signifi-

cantly higher than those found in the Red bed groundwater samples. Inversely, the Coefficients of Variation (CV) for the chemical parameters in the red bed groundwater were much higher than those in geothermal water. As shown in Table 2, indicators with CV values greater than 1 in the Red bed groundwater included Na^+, K^+, Cl^-, SO_4^{2-}, NO_3^-, and F^-, demonstrating that the values of these parameters were highly variable.

Pearson's correlation analysis was conducted to explore the relationships among the chemical components of water. Significant positive correlations were observed between most anions and cations in the Red bed groundwater. For instance, Cl^- and Na^+ showed a strong correlation ($r^2 = 0.97$, $p < 0.01$), as did SO_4^{2-} with Na^+, Ca^{2+} ($r^2 = 0.73$, 0.60, $p < 0.01$), and HCO_3^- with Ca^{2+} and Mg^{2+} ($r^2 = 0.48$, 0.53, $p < 0.01$) (Fig. 3). These findings indicate that the ions primarily originate from the dissolution of carbonate rocks, sulfate minerals, and salt rocks in the Red bed. On the contrary, the correlations between anions and cations in geothermal water revealed significant positive correlations between SO_4^{2-} and Ca^{2+}, Mg^{2+} ($r^2 = 0.85$, 0.73, $p < 0.01$), and between F^- and K^+ ($r^2 = 0.80$, $p < 0.01$), suggesting that the water chemistry in the geothermal environment is more strongly influenced by the dissolutions of sulfate and fluoride. Furthermore, there are notable differences in the correlations between F^- and other ions in the red bed groundwater and geothermal water. Moderate positive correlations ($r^2 = 0.64$, 0.59, 0.45, $p < 0.01$) were found between F^- with Na^+, Cl^-, and SO_4^{2-} in the Red bed groundwater, suggesting common sources such as salt rocks or sulfate
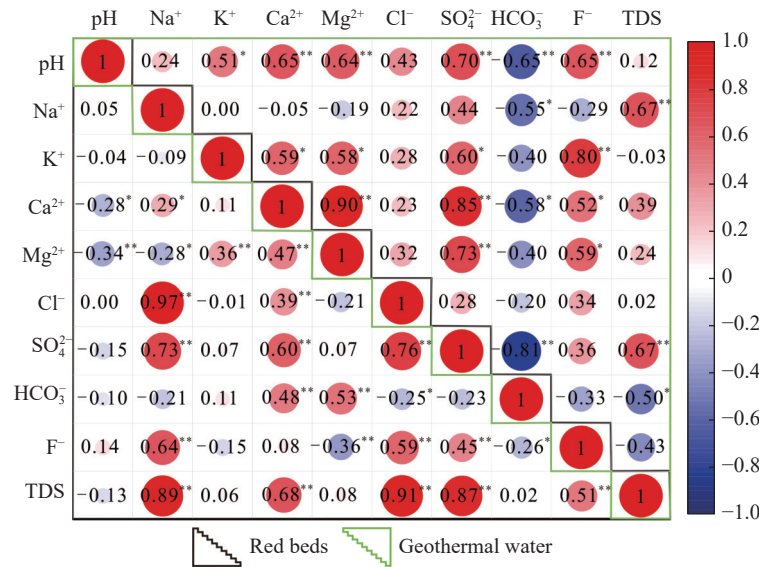
Fig. 3 Correlation coefficients of the major water parameters and elements in Red beds (n=68) and geothermal water (n=17)

(Note：** P < 0.01; * P < 0.05)

minerals. Previous studies have indicated that higher TDS enhances strength of the solution, leading to increased solubility of fluoride (Chae et al. 2007). The moderate positive correlation ($r^2 =$ 0.51, p < 0.01) between F^- and TDS in the Red bed groundwater suggested that an increase in TDS, possibly caused by evaporation or mineral dissolution, may contribute to the enrichment of F^-. In contrast, F^- showed no significant correlation with TDS in the geothermal water. However, positive correlations ($r^2 = 0.80$, 0.89, 0.52, p < 0.05) between F^- and K^+, Ca^{2+}, and Mg^{2+} suggested that F^- may be associated with the dissolution of fluorspar minerals in the geothermal environment. The similar ionic radii and charges of OH^- and F^- suggest that OH^- can displace F^- adsorbed on the lattice surface of the minerals, thereby promoting desorption of fluorine-containing minerals (Lia et al. 2021). Consequently, the positive correlation between fluorine content and pH in geothermal water suggests that an alkaline environment is favorable for the enrichment of F^-.

3.2 Chemical types of groundwater

The Piper diagram, which plots the scatter of anions (HCO_3^-, Cl^-, and SO_4^{2-}) and cations (Na^+, K^+, Ca^{2+}, and Mg^{2+}), is commonly used to represent the chemical compositions of groundwater (Lan et al. 2024; Piper, 1944). To better understand the hydrochemical characteristics of fluoride in the groundwater, the samples were classified into two categories: Highly fluoridated groundwa-

ter ($F^- \geq 1$ mg·L^{-1}) and low fluoridated groundwater ($F^- < 1$ mg·L^{-1}). In the geothermal water, the milligram equivalents of Na^++K^+, Ca^{2+}, and Mg^{2+} accounted for approximately 0–10%, 90%–100%, and 20%–35% of the total cations, respectively. Meanwhile, the milligram equivalents of HCO_3^-, Cl^-, and SO_4^{2-} mostly accounted for 5%–40%, 0–15%, and 60%–95% of the total anions, respectively (Fig. 4). This composition indicated that the geothermal water is predominantly composed of the cation Ca^{2+} and the anion SO_4^{2-}, categorizing it primarily as SO_4-Ca type. Conversely, low-F^- red bed groundwater was prominently composed of Ca^{2+} and HCO_3^- ions, classifying it primarily as HCO_3-Ca type. High-F^- red bed groundwater, on the other hand, contained Na^+, Cl^-, or HCO_3^- ions
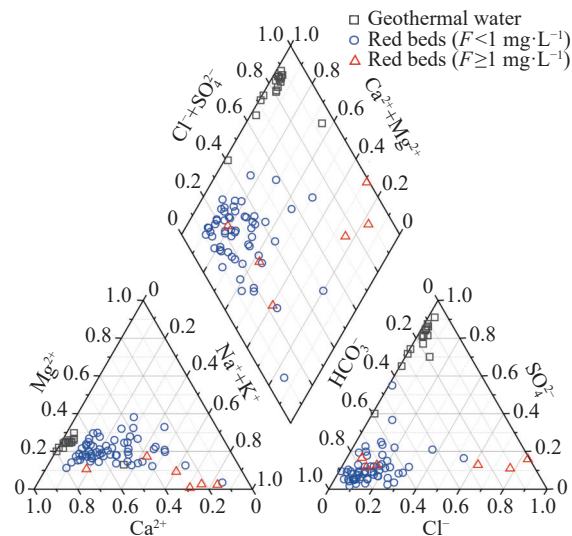

Fig. 4 Piper plots of water samples in the study area

as the major constituents, primarily classifying it as either Cl-Na, HCO$_3$-Na, or HCO$_3$-Na·Ca type.

4 Discussion

4.1 Rock weathering and F contents in different rocks

Based on an analysis of the water chemistry of numerous global surface waters, Gibbs proposed diagrams (Fig. 5a) to comprehensively explain the chemistry and genesis of water, highlighting three primary factors that influence water chemistry composition: Evaporation dominance, rock dominance, and precipitation dominance (Gibbs, 1970).

The geothermal water and low-F$^-$ Red bed groundwater samples clustered within the rock dominance corner of the Gibbs diagrams (Figs 5b and 5c), with the ratios of Cl$^-$/(Cl$^-$+HCO$_3^-$) and Na$^+$/(Na$^+$+Ca^{2+}) ranging from 0.18 to 0.87 and from 0.13 to 0.99, respectively. On the other hand, half of the red bed groundwater with high F$^-$ concentration had both higher TDS levels and higher ratios of Cl$^-$/(Cl$^-$+HCO$_3^-$) and Na$^+$/(Na$^+$+Ca^{2+}). These samples were located at the evaporation domi-

nance endmember, while the other half fell within the rock dominance zone (Figs 5b and 5c). The results indicated that the major compositions of most groundwater samples were influenced by rock weathering. Only a small portion of the red bed groundwater samples with high F$^-$ content might be affected by evaporation processes or dissolution of soluble salts, such as halite and sylvite.

The F contents in rocks from the studied region exhibited significant variation (Table 3). Most rock samples contained fluorine levels exceeding the average background value in the continental crust (525 mg·kg^{-1}) (Wedepohl, 1995). Among the rock types, marl, mudstone, carbonaceous mudstone, and siltstone exhibited particularly high average F$^-$ contents, at 767 mg·kg^{-1}, 722 mg·kg^{-1}, 705 mg·kg^{-1}, and 671 mg·kg^{-1}, respectively. These values were higher compared to basalt (645 mg·kg^{-1}), sandstone (423 mg·kg^{-1}), and limestone (365 mg·kg^{-1}). Previous studies have highlighted that fine-grained particles, such as those found in mudstone and siltstone, possess a large specific surface area with abundant adsorption sites, enabling them to adsorb fluoride ions effectively
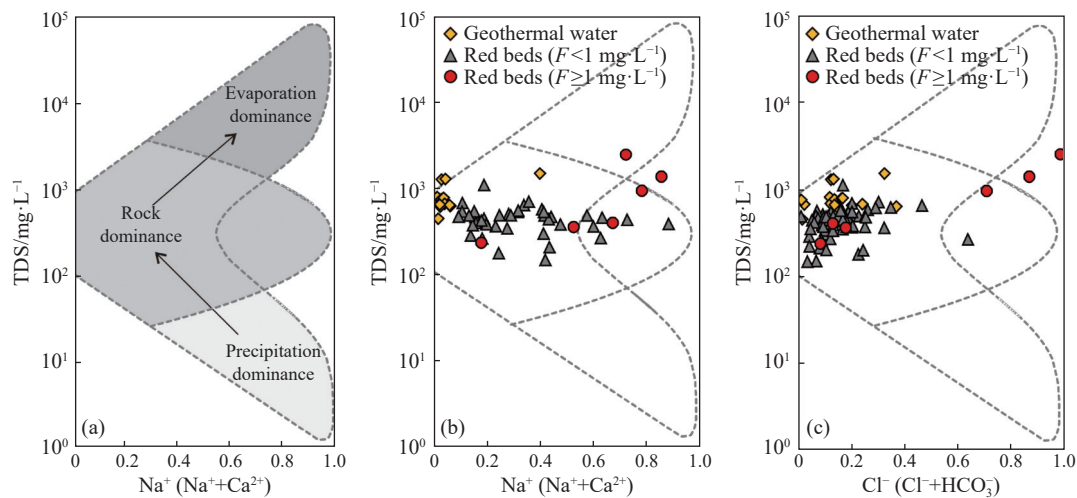

Fig. 5 Gibbs plots: (a) Comparison of natural processes that define the water chemistry of water on the Gibbs plots; (b) TDS versus Na$^+$/(Na$^+$+Ca^{2+}); (c) TDS versus Cl$^-$/(Cl$^-$+HCO$_3^-$)

Table 3 F contents in the various rocks of the study area/(mg·kg^{-1})

Rock type	Marl (*n*=2)	Limestone (*n*=6)	Mudstone (*n*=8)	Carbonaceous mudstone (*n*=3)	Siltstone (*n*=3)	Sandstone (*n*=4)	Basalt (*n*=1)	All samples (*n*=27)
Min	767	200	598	542	645	408	645	200
Max	767	476	854	767	767	476	645	854
Ave	767	365	722	671	705	432	645	593
SD	-	122	80	116	61	30	-	178
Average value of continental crust (Wedepohl, 1995)	525							

(Dey et al. 2012; Jacks et al. 2005; Zhu et al. 2015). Consequently, rocks with high-fluoride content may act as source materials contributing to the development of high-fluoride groundwater in certain areas of the red bed region.

4.2 Mineral dissolution

As previously discussed, mineral weathering in rocks, along with evaporation, may contribute to the presence of fluoride in groundwater. Fig. 1 illustrates that soluble minerals such as calcite, gypsum, fluorite, halite, and sylvite play a significant role in the water-rock interactions within the strata of the study area. The Saturation Index (*SI*) of minerals was used to analyze the hydrochemical evolution of various dissolved minerals in the groundwater environment (Güler and Thyne, 2004). It was calculated using the following equation (Kammoun et al. 2022):

$$SI = \lg \frac{IAP}{K} \qquad (3)$$

Where: *K* represents the equilibrium constant, and *IAP* is the ion activity product. The mineral does not reach solvation equilibrium when *SI* < 0. When *SI* > 0, the corresponding mineral is supersaturated and may have precipitated. When *SI* = 0, the mineral reaches a relatively stable equilibrium condition.

The saturation indices for calcite, fluorite, gypsum, halite, and sylvite in the groundwater are summarized in Table 4. The results revealed that halite and sylvite were significantly undersaturated, with the *SI* values ranging from −10.12 to −4.84 for halite and −9.65 to −6.48 for sylvite, respectively. For calcite, the *SI* values in the red bed groundwater and geothermal water ranged from −1.88 to 1.18 and from −0.27 to 1.00, with mean values of 0.03 and 0.04, respectively. Only a

minimal number of geothermal water samples were found to be saturated with gypsum, with *SI* values ranging from −0.82 to −0.09. The findings suggested that these minerals were approaching a near-saturation state. The *SI* values for fluorite in the geothermal water showed significant variation across different water types. In geothermal water, low-F⁻ Red bed groundwater, and high-F⁻ Red bed groundwater, the *SI* values ranged from −2.66 to 1.80, from −4.00 to −1.03, and from −0.96 to 0.24, with mean values of 0.78, −2.00, and −0.37, respectively. Notably, both geothermal water and high-F⁻ red bed groundwater were nearly saturated with fluorite, indicating that dissolution of fluorite serves as a primary source of F⁻ in the groundwater.

To further investigate the relationship between fluoride concentration and the saturation indices of minerals, scatter plots of these indicators are presented in Fig. 6. A power exponent ($y = 2.37 \times e^{0.98x}$, $r = 0.97$) between fluoride concentration and the *SI*-fluorite value demonstrates that fluorite dissolution significantly impacts the enrichment of F⁻. Furthermore, the oversaturation state of fluorite may not appear to impose a limiting effect on the increase in F⁻ content (Fig. 6a). Bubble charts (Figs 6b, 6c, and 6d) showed that the bubble sizes, representing fluoride content, do not exhibit a clear increasing trend with the saturation indices of these minerals, except for fluorite. This finding implied that the dissolution of gypsum, calcite, and halite may not directly impact the fluoride concentration. Most calcite in the red bed groundwater is supersaturated, indicating that the precipitation of calcite formed by Ca²⁺ likely promotes the dissolution of fluorite (Fig. 6b).

Scatter plots of the activities of F⁻ and Ca²⁺ were used to ascertain the proportions of carbonate and fluorite dissolved in the aqueous environments (Fig. 7) (Lyu et al. 2021; Mao et al. 2016). The

Table 4 Statistics of groundwater mineral saturation indices in the study area

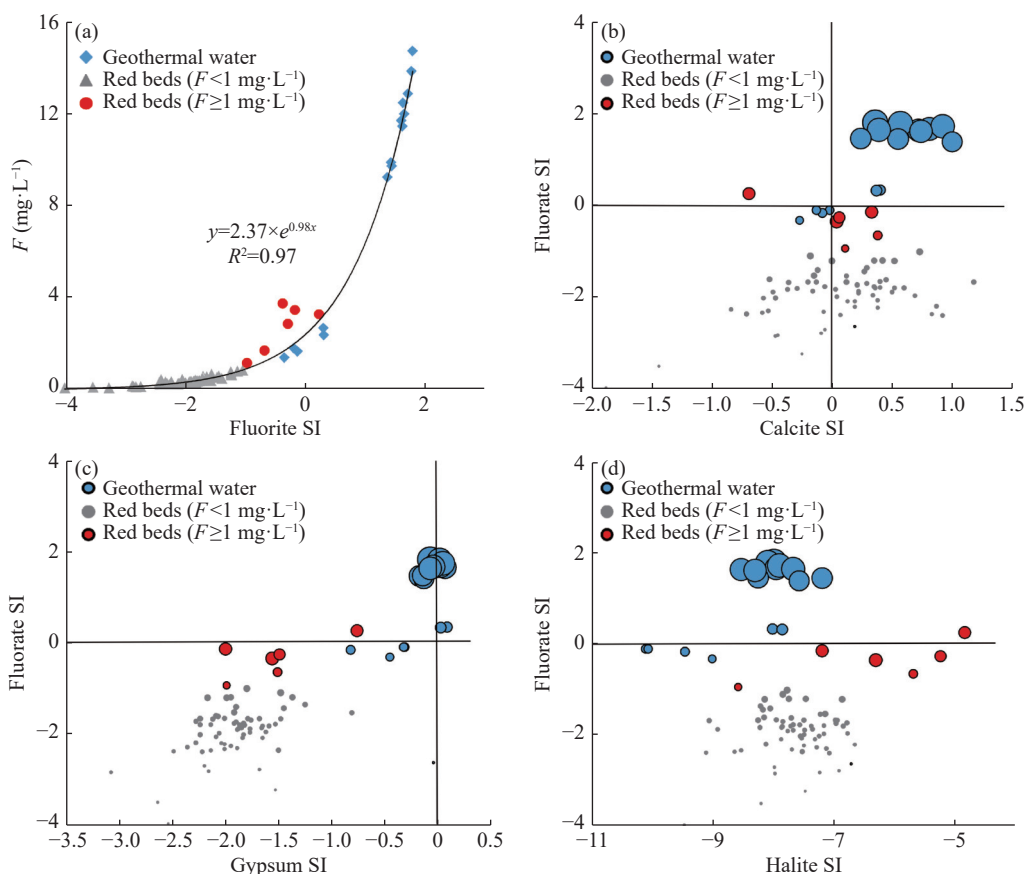| Mineral category			Calcite (CaCO₃)	Fluorite (CaF₂)	Gypsum (CaSO₄·2H₂O)	Halite (NaCl)	Sylvite (KCl)
Geothermal water (n=17)		Max	1.00	1.80	0.09	−6.72	−7.23
		Min	−0.27	−2.66	−0.82	−10.12	−9.65
		Ave	0.40	0.78	−0.13	−8.28	−8.11
Red beds (n=68)	Low F⁻ level (n=62)	Max	1.18	−1.03	−0.81	−6.66	−6.48
		Min	−1.88	−4.00	−3.08	−9.48	−9.90
		Ave	0.03	−2.00	−1.91	−7.67	−8.33
	High F⁻ level (n=6)	Max	0.38	0.24	−0.76	−4.84	−7.05
		Min	−0.69	−0.96	−2.00	−8.59	−8.94
		Ave	0.04	−0.37	−1.55	−6.31	−7.92

Fig. 6 Saturation indices of minerals: (a) F⁻ vs. *SI*-fluorite, (b) *SI*-fluorite vs. *SI*-calcite, (c) *SI*-fluorite vs. *SI*-gypsum, and (d) *SI*-fluorite vs. *SI*-halite (The bubble sizes represent the F⁻ concentration)

calculation of ion strength and ion activity in the solution was performed using the Debye–Hückel equations (Silva et al. 2022):

$$-\lg\gamma_i = 0.51z_i^2\left(\sqrt{I}/(1 + B\acute{a}\sqrt{I})\right) \qquad (4)$$

$$I = 0.5\sum(c_i \times z_i^2) \qquad (5)$$

Fig. 7 The relationship between the activities of F⁻ and Ca²⁺ of the groundwater in the study area

$$\lg[i]_{activity} = log_{10}(\gamma_i \times c_i) \qquad (6)$$

Where: γ_i represents the activity coefficient of ion i in solution, z_i is the charge of ion i, I is the ionic strength of the solution, and B is a constant (0.00328 at 25°C). The symbol $\acute{a}$ refers to the effective radius of the hydrated ion, measured in units of 10^{-12} m. c_i is the concentration of the ion i. The term $\lg[i]_{activity}$ represents the logarithmic form of the ion activity. When only fluorite is dissolved, the activities of Ca²⁺ and F⁻ in solution predominantly align near line 1. When the dissolved mass ratio of calcite to fluorite is 200:1, the activities of Ca²⁺ and F⁻ primarily cluster around the trend line 2. Additionally, when cation exchange or calcite precipitation occurs, the activities of Ca²⁺ and F⁻ coincide with the range of line 3 (Lyu et al. 2021; Mao et al. 2016). The activities of fluorine and calcium in the groundwater are displayed in Fig. 7. Most high-F⁻ Red bed groundwater samples and geothermal water samples plotted above or near the fluorite dissolution equilibrium line (lg*K* = 10.6), indicating that the fluorite dissolution in these water bodies was oversaturated or near-saturated. The low-F⁻ red bed groundwater samples were predominantly near line 2, indicating that

carbonate dissolution greatly exceed fluorite dissolution. In addition, the high-F^- red bed groundwater and geothermal water samples plotted between line 1 and line 2, suggesting that cation exchange or calcite precipitation may positively influence the fluorite dissolution mechanism in the groundwater.

4.3 Cation exchange

Cation exchange is a significant process that dominate the ionic composition in groundwater and plays a crucial role in the formation of water hydrochemistry during water-rock interactions (Yan and Feng, 2022). The chloro-alkaline indices (CAI1 and CAI2) are commonly used to assess cation exchange processes in groundwater (Schoeller, 1967; Zhang et al. 2024). The calculations of these indices are as follows:

$$CAI1 = [Cl^- - (Na^+ + K^+)]/Cl^- \qquad (7)$$

$$CAI2 = [Cl^- - (Na^+ + K^+)]/$$
$$(SO_4^{2-} + HCO_3^- + CO_3^{2-} + NO_3^-) \qquad (8)$$

Where: The ions represent the molar concentration of the corresponding component. The values of CAI1 and CAI2 are positive when Na^+ and K^+ in the groundwater displace adsorbed Ca^{2+} and Mg^{2+} in the aquifer. Conversely, negative values indicate the reverse process. Moreover, the magnitude of the absolute values of CAI1 and CAI2 reflects the intensity of the cation exchange process, with larger absolute values indicating stronger cation exchange.

As shown in Fig. 8a, the chloro-alkaline indices (CAI1 and CAI2) were almost negative, indicating that Ca^{2+} and Mg^{2+} in the water likely exchanged with Na^+ and K^+ in adsorbed states. Notably, two

anomalies were observed in Fig. 8a, which may be related the increase of Na^+ content in groundwater caused by either cation exchange processes or human activities. Excluding these anomalies, the CAI1 and CAI2 values in geothermal water varied from −5.41 to 0.05 and from −0.09 to −0.01, respectively, while those in the red bed groundwater ranged from −18.59 to 0.211 and from −0.87 to 0.23, respectively. The greater variability in CAI1 and CAI2 values observed in the red bed groundwater suggests that stronger cation exchange processes might occur within the water-rock environment. Moreover, the Red bed groundwater samples with higher fluoride contents tended to be located relatively distant from the origin of the axes, suggesting that cation exchange may play a role in facilitating the fluorine enrichment in groundwater.

The diagram of $\gamma((Ca^{2+}+Mg^{2+})-(HCO_3^- + SO_4^{2-}))$ as a function of $\gamma(K^+ +Na^+ -Cl^-)$ provides a clearer understanding of the occurrence of cation exchange in groundwater (Xiao et al. 2016). A linear correlation with a slope of −1.0 is expected when cation exchange dominates the water's chemical composition. According to Fig. 8b, the negative correlation between $\gamma((Ca^{2+}+Mg^{2+})-(HCO_3^-+ SO_4^{2-}))$ and $\gamma(K^++Na^+-Cl^-)$ ($y = -1.13x + 0.52$, $r^2 = 0.76$) in the Red bed groundwater suggested a significant cation exchange process. Additionally, most of the red bed groundwater samples were plotted in the fourth quadrant of the diagram (Fig. 8b), demonstrating that an increase in Na^+ and K^+ corresponded to a decrease in Ca^{2+} and Mg^{2+} in the groundwater. The cation exchange equation in the red bed groundwater can be represented as: Na_4-aqueous medium + $(Ca^{2+} + Mg^{2+})$-groundwater $\leftrightarrow$ $4Na^+$-groundwater + (Ca + Mg)-aqueous medium
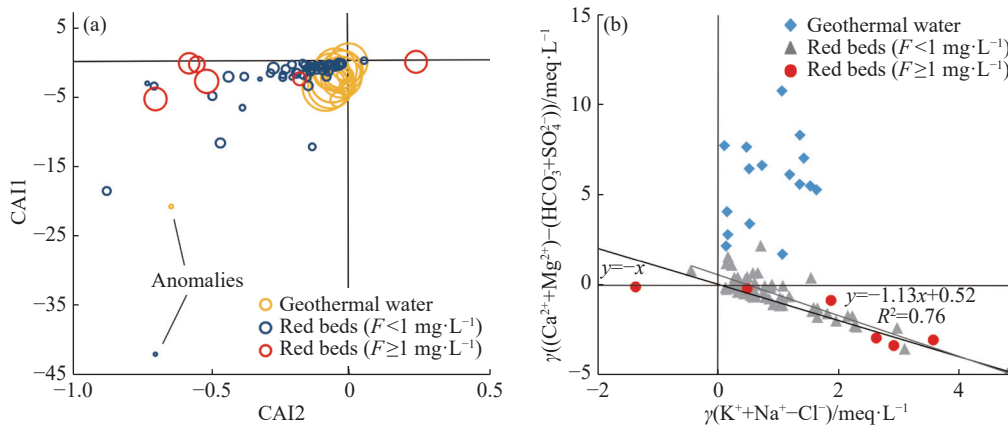

Fig. 8 (a) Relationship between CAI1 and CAI2 in the groundwater sample (the bubble size corresponds to the concentration of fluoride in the sample); (b) Relationships between $\gamma((Ca^{2+}+Mg^{2+})-(HCO_3^- + SO_4^{2-}))$ and $\gamma(K^+ +Na^+ -Cl^-)$ in groundwater

(Sikdar et al. 2001).

In contrast, the geothermal water points plotted in the first quadrant of the diagram, which may suggest the concurrent mineral dissolution in the geothermal environment. This indicates that the cation exchange process significantly influences the chemistry of Red bed groundwater, particularly causing an increase in Na^+ and K^+ levels while depleting Ca^{2+} and Mg^{2+} concentrations.

Previous studies have showed that a high-Na and low-Ca groundwater environment promotes the enrichment of fluoride in groundwater for two primary reasons. First, the low concentration of Ca^{2+} facilitates the dissolution of fluorite. Second, environments with elevated Na^+ levels and reduced Ca^{2+} and Mg^{2+} concentrations exhibits a decrease in the adsorption charge on the surface of Al/Fe hydroxides, enhancing the desorption of anions, including fluoride (Aghapour et al. 2018; Li et al. 2015).

4.4 The formation model of high-F^- groundwater

The significant disparities in water chemistry between the geothermal water and red bed groundwater suggest that the high fluorine content in the geothermal water from the adjacent fold belt is unlikely to be the primary source of fluorine in the red bed groundwater. As previously discussed, the high-F^- Red bed groundwater is predominantly of the Cl-Na or HCO_3-Na type, characterized by Na-enriched and Ca-depleted conditions, whereas the high-fluoride geothermal water is mainly SO_4-Ca type, characterized by Ca-enriched and Na-depleted conditions (Fig. 9a). Furthermore, the hydrochemistry of geothermal water is closely associated with fluorite and sulfate minerals in the fold belt region, which is rich in geothermal resources (Li et al. 2020; Qian et al. 2012).

However, this association is not characteristic of the water-rock environment in the Red bed area, which is characterized by relatively thick and horizontally bedded layers (Xie et al. 1981).

The investigated region is a typical agricultural area characterized by purple soil and minimal animal husbandry (Lei and Liu, 2022). Generally, NO_3^- in groundwater primarily originates from agricultural activities, and the correlation between NO_3^- content and other components can provide insight into the role of agriculture (Li et al. 2015). As shown in Fig. 9b, little correlation was observed between NO_3^- and F^- in the Red bed groundwater. Samples with F^- concentrations greater than 1 mg/L had NO_3^- concentrations ranging from ND to 47.5 mg/L, while the F^- concentration did not exceed 0.5 mg/L in samples with NO_3^- concentrations greater than 100 mg/L (Fig. 9b). These results indicate that regional agricultural activities have a limited impact on F^- content in groundwater, and the application of nitrogen fertilizers in agriculture not significantly contribute to F^- enrichment.

Based on the previous discussion, the genetic model of high-fluorine groundwater in the study area is illustrated in Fig. 10. Groundwater in the red bed area is replenished primarily by rivers and atmospheric rainfall. From the regional geology and the Red bed geological profile of the Guang'an area (Figs 1b and 1c), it is evident that the sandstone layers exhibit good permeability, facilitating groundwater flow. However, the presence of near-horizontal strata and shale interlayers can lead to the development of localized aquifers with slow flow (Fig. 10). Studies have indicated that areas with rapid groundwater flow are less conducive to fluoride enrichment, while regions with slow water movement and significant evaporation are more likely to experience fluorine enrichment in the epigenetic geochemical environment (Durrani and
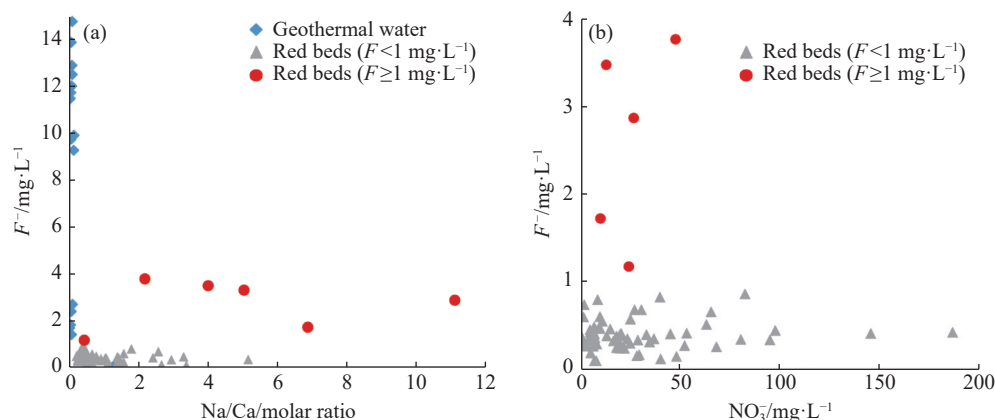

Fig. 9 Relationships between Na/Cl and F^- (a) and between NO_3^- and F^- (b) in groundwater from the study area
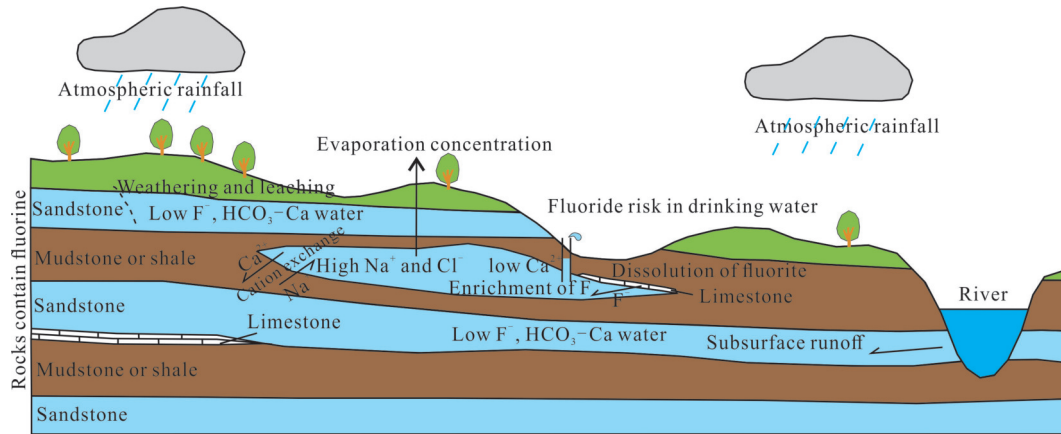
Fig. 10 Genetic model of high-fluoride groundwater in the study area

Farooqi, 2021; Jacks et al. 2005). As shown in Fig. 10, most groundwater in red beds experiences rapid recharge from precipitation or river water. Analysis using Piper plots (Fig. 4), Gibbs plots (Fig. 5), and mineral saturation characteristics (Fig. 6) indicates that groundwater in such areas is predominantly influenced by atmospheric CO_2, along with the weathering and dissolution of carbonate minerals, resulting in HCO_3-Ca type water with a low fluoride content. On the other hand, red bed aquifers with slow groundwater regeneration and relatively confined conditions, experience processes such as cation exchange, slow evaporation, and concentration, leading to an increase in Na^+ and Cl^-, and a decrease in Ca^{2+} (Fig. 10). These conditions promote the formation of Cl-Na or HCO_3-Na type water, creating favorable conditions for fluorine enrichment. Additionally, the analyzed rock data suggest that the marl or paste rock interlayers in the red bed area contain abundant fluorine minerals (Table 3), which can act as a source of fluoride in groundwater. Therefore, the formation of high-fluorine groundwater in red beds are similar to those found in many arid regions, basins, or plains, which often exhibit poor hydrodynamic conditions, shallow water tables, and processes of evaporation and concentration

(Su et al. 2021; Zhang et al. 2023).

4.5 Health risk assessment of fluoride dissemination

The Hazard Quotient (*HQ*) of fluoride in drinking water is presented in Figs 11a and 11b. For children, the Hazard Quotient (*HQ*) values in the Red bed groundwater ranged from 0.10 to 4.70, with an average value of 0.73 (Fig. 11a). For adults, the *HQ* values were in the range of 0.07–3.13, with a mean of 0.48 (Fig. 11b). There are limited reports indicating the direct use of this groundwater for drinking purposes in the development of natural mineral water. Consequently, the geothermal water is excluded for the health risk assessment for fluoride exposure. Among the sampled red bed groundwater points, 7% (n = 5) and 12% (n = 8) exceeded the Recommended reference Dose (*RfD*) for adults and children, respectively. This highlights that children are at a greater risk of adverse health effects from fluoride exposure through water consumption compared to adults. The spatial distribution of *HQ* values in the red bed groundwater was non-uniform and lacked a clear spatial pattern. However, the variation in *HQ* values
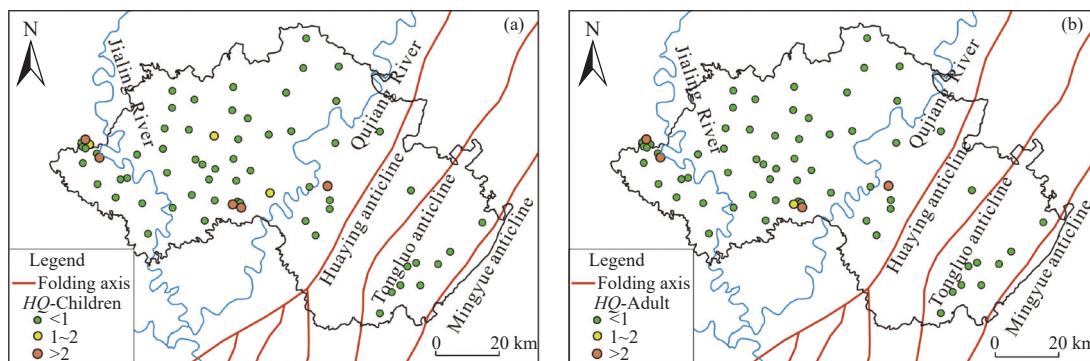

Fig. 11 Noncarcinogenic evaluation for fluoride concentrations in Red bed groundwater: (a) Children and (b) Adults

aligned closely with the spatial distribution of groundwater fluorine concentrations.

Purple soil, developed from red beds, is a crucial component of agricultural cultivation, supporting the production of fruits, vegetables, grains, and oils (Qian et al. 2012). Red bed groundwater plays an essential role in sustaining local livelihoods, agriculture, and industrial development. Therefore, mitigating the health risks posed by high-fluoride water is a pressing concern for local governments. Measures should be implemented to avoid the extraction of groundwater from aquifers with elevated fluoride concentrations. Additionally, it is crucial to enhance the monitoring of groundwater quality across various aquifers and, where necessary, utilize standardized water treatment methods to reduce fluoride levels.

5 Conclusions

The causes and noncarcinogenic risks associated with fluoride in the red bed groundwater and the adjacent geothermal water of the Guang'an area were comprehensively investigated, leading to the following conclusions:

(1) High-fluoride samples constitute approximately 9% of the total Red bed groundwater, with the primary hydrochemical types being Cl-Na and HCO_3-Na. In contrast, low-fluoride groundwater predominantly exhibits an HCO_3-Ca hydrochemical type. In geothermal water, about 94% of the samples are high-fluoride, primarily characterized by the SO_4-Ca type. Correlation analysis of fluoride and other chemical indicators revealed that the source of fluoride in Red bed groundwater is unrelated to the neighboring geothermal water.

(2) Fluoride in Red bed groundwater originates primarily from fluorine-rich rocks. Key natural factors influencing fluoride enrichment include geological structure, rock weathering, evaporation and concentration, cation exchange, and mineral saturation. This process differs significantly from the high-fluoride groundwater in geothermal environments in neighboring regions.

(3) Based on the noncarcinogenic health risk evaluation, 7% and 12% of Red bed groundwater samples exceeded the recommended reference dose for adults and children, respectively. Since fluoride is a crucial indicator of groundwater safety, it is advisable to avoid extracting water from high-fluoride aquifers. Regular monitoring of groundwater quality and the implementation of standardized water treatment methods are necessary to mitigate health risks.

Acknowledgements

References

Aghapour S, Bina B, Tarrahi MJ, et al. 2018. Distribution and health risk assessment of natural fluoride of drinking groundwater resources of Isfahan, Iran, using GIS. Environmental Monitoring and Assessment, 190: 137. DOI：10.1007/s10661-018-6467-z.

Ali S, Thakur SK, Sarkar A, et al. 2016. Worldwide contamination of water by fluoride. Environmental Chemistry Letters, 14(3): 563−568. DOI：10.1007/s10311-016-0563-5.

Chae GT, Yun ST, Mayer B, et al. 2007. Fluorine geochemistry in bedrock groundwater of South Korea. Science of the Total Environment, 385(1-3): 272−283. DOI：10.1016/j. scitotenv.2007.06.038.

Chen JN, Mao XG, Shi YH, et al. 2020. Study on the late Cretaceous paleoenvironment documented by red beds in the western Fujian province. Chinese Journal of Geophysics, 63(4): 1553−1568. DOI：10.6038/cjg2020N0375.

Dey RK, Swain SK, Mishra S, et al. 2012. Hydrogeochemical processes controlling the high fluoride concentration in groundwater: A case study at the Boden block area, Orissa, India. Environmental Monitoring and Assessment, 184(5): 3279−3291. DOI：10.1007/s10661-011-2188-2.

Dong JX, Sun D, Wei LS, et al. 2021. Discussion on the development regularity of salt water in red beds in the southern margin of Sichuan Basin. Geological Bulletin of China, 40(8): 1394−1401. (in Chinese)

Duan X. 2015. Highlights of the Chinese exposure factors handbook (adults). Academic Press. (in Chinese)

Durrani TS, Farooqi A. 2021. Groundwater fluoride concentrations in the watershed sedimentary basin of Quetta Valley, Pakistan. Environmental monitoring and assessment, 193(10): 644. DOI：10.1007/s10661-021-09365-8.

Feng F, Jia YF, Yang Y, et al. 2020. Hydrogeochemical and statistical analysis of high fluo-

ride groundwater in northern China. Environmental Science and Pollution Research, 27(28): 34840−34861. DOI：10.1007/s11356-020-09784-z.

Gao ZJ, Zhu ZH, Liu XD, et al. 2014. The formation and model of high fluoride groundwater and in-situ dispelling fluoride assumption in Gaomi City of Shandong Province. Journal of Groundwater Science and Engineering, 2(2): 34−39. DOI：10.26599/JGSE.2014.9280016.

Gibbs RJ. 1970. Mechanisms controlling world water chemistry. Science, 170(3962): 1088−1090. DOI：10.1126/science.170.3962.1088.

Güler C, Thyne GD. 2004. Delineation of hydrochemical facies distribution in a regional groundwater system by means of fuzzy c-means clustering. Water Resources Research, 40(12): W12503. DOI：10.1029/2004wr003299.

Hao AB, Zhang YL, Zhang EY, et al. 2018. Review: Groundwater resources and related environmental issues in China. Hydrogeology Journal, 26(5): 1325−1337. DOI：10.1007/s10040-018-1787-1.

He XD, Li PY, Ji YJ, et al. 2020. Groundwater Arsenic and Fluoride and Associated Arsenicosis and Fluorosis in China: Occurrence, Distribution and Management. Exposure and Health, 12(3): 355−368. DOI：10.1007/s12403-020-00347-8.

Jacks G, Bhattacharya P, Chaudhary V, et al. 2005. Controls on the genesis of some high-fluoride groundwaters in India. Applied Geochemistry, 20(2): 221−228. DOI：10.1016/j.apgeochem.2004.07.002.

Jia H, Qian H, Qu W, et al. 2019. Fluoride occurrence and human health risk in drinking water wells from southern edge of Chinese Loess Plateau. International Journal of Environmental Research and Public Health, 16(10): 1683−1695. DOI：10.3390/ijerph16101683.

Kammoun A, Abidi M, Zairi M. 2022. Hydrochemical characteristics and groundwater quality assessment for irrigation and drinking purposes: A case of Enfidha aquifer system, Tunisia. Environmental Earth Sciences, 81(41): 1−10. DOI：10.1007/s12665-021-10163-1.

Khatri N, Tyagi S. 2015. Influences of natural and anthropogenic factors on surface and groundwater quality in rural and urban areas. Frontiers in Life Science, 8(1): 23−39. DOI：10.1080/21553769.2014.933716.

Kumar M, Goswami R, Patel AK, et al. 2020. Scenario, perspectives and mechanism of arsenic and fluoride Co-occurrence in the groundwater: A review. Chemosphere, 249(12): 2−20. DOI：10.1016/j.chemosphere.2020.126126.

Lan FN, Zhao Y, Li J, et al. 2024. Health risk assessment of heavy metal pollution in groundwater of a karst basin, SW China. Journal of Groundwater Science and Engineering, 12(1): 49−61. DOI：10.26599/jgse.2024.9280005.

Lei FH, Liu CZ. 2022. Report of geochemical survey of land quality in Guang'an City: Chengdu Geological Survey Center, China Geological Survey. (in Chinese)

Li CC, Gao XB, Wang YX. 2015. Hydrogeochemistry of high-fluoride groundwater at Yuncheng Basin, northern China. Science of the Total Environment, 508(1): 155−165. DOI：10.1016/j.scitotenv.2014.11.045.

Li MH, Yuan JF, Huang CJ, et al. 2020. A study of the characteristics of geothermal reservoir and genesis of thermal groundwater in the Tongluoshan anticline near Guang'an in east Sichuan. Hydrogeology & Engineering Geology, 47(6): 36−46. (in Chinese) DOI：10.16030/j.cnki.issn.1000-3665.202008038.

Lia Q, Tao HF, Aihemaiti M, et al. 2021. Spatial distribution characteristics and enrichment factors of high-fluorine groundwater in the Kuitun River Basin of Xinjiang Uygur Autonomous Region in China. Desalination and Water Treatment, 223: 208−217. DOI：10.5004/dwt.2021.27138.

Liu RP, Liu F, Chen HQ, et al. 2024. Arsenic and fluoride co-enrichment of groundwater in the loess areas and associated human health risks: A case study of Dali County in the Guanzhong Basin. China Geology, 7(3): 445−459. DOI：10.31035/cg2024015.

Liu RP, Zhu H, Liu F, et al. 2021. Current situation and human health risk assessment of fluoride enrichment in groundwater in the Loess Plateau: A case study of Dali County, Shaanxi Province, China. China Geology, 4(3): 487−497. DOI：10.31035/cg2021051.

Lyu XL, Liu JT, Zhou B, et al. 2021. Distribution characteristics and enrichment mechanism of fluoride in the shallow aquifer of the Tacheng Basin. Earth Science Frontiers, 28(2): 426−436. (in Chinese) DOI：10.13745/j.esf.sf. 2020.10.29.

Luo JL. 2020. Regional distribution characteristies and genesis analysis of fluorinecontent in groundwater in South Jiangxi. Mineral Resources and Geology, 34(3): 590−595. (in Chinese) DOI：10.19856/j.cnki.issn.1001-5663.2020.03.026.

Mao RY, Cuo HM, Jia YF. 2016. Distribution characteristics and genesis of fluoride groundwater in the Hetao basin, Inner Mongolia. Earth Science Frontiers, 23(2): 260−268. (in Chinese) DOI：10.13745/j.esf.2016.02.024.

Piper M. 1944. A graphic procedure in the geochemical interpretation of water-analyses. Transactions-American Geophysical Union, 25(6): 914−923. DOI：10.1029/TR025i0 06p00914.

Podgorski J, Berg M. 2022. Global analysis and prediction of fluoride in groundwater. Nature Communications, 13(1): 4232. DOI：10.1038/s41467-022-31940-x.

Qian LJ, Chen HD, Lin LB, et al. 2012. Geochemical characteristics and environmental implications of Middle Jurassic Shaximiao Formation, western margin of Sichuan Basin. Acta Sedimentologica Sinica, 30(6): 1061−1071. (in Chinese) DOI：10.14027/j.cnki.cjxb.2012. 06.020.

Schoeller H. 1967. Qualitative evaluation of groundwater resources. In methods and technics of groundwater investigation and development. Water Research, 33: 44−52.

Sheldon ND. 2005. Do red beds indicate paleoclimatic conditions? A Permian case study. Palaeogeography, Palaeoclimatology, Palaeoecology, 228(3-4): 305–319. DOI：10.1016/j. palaeo.2005.06.009.

Sikdar PK, Sarkar SS, Palchoudhury S. 2001. Geochemical evolution of groundwater in the Quaternary aquifer of Calcutta and Howrah, India. Journal of Asian Earth Sciences, 19(5): 579−594. DOI：10.1016/s1367-9120(00) 00056-0.

Silva GM, Liang X, Kontogeorgis GM. 2022. On the derivations of the Debye–Hückel equations. Molecular Physics, 120(10): 1−22. DOI：10.1080/00268976.2022.2064353.

Su H, Kang WD, Kang N, et al. 2021. Hydrogeochemistry and health hazards of fluoride-enriched groundwater in the Tarim Basin, China. Environmental Research, 200(3): 111−130. DOI：10.1016/j.envres.2021. 111476.

USEPA. 1987. Integrated Risk Information System, Chemical Assessment Summary, Fluorine (soluble fluoride); CASRN 7782-41-4. Available on https://iris.epa.gov/static/pdfs/ 0053_summary.pdf.

Wedepohl KH. 1995. The composition of the continental crust. Geochimica et Cosmochimica Acta, 59(7): 1217−1232. DOI：10.1016/ 0016-7037(95)00038-2.

Wen DG, Zhang FC, Zhang EY, et al. 2013. Arsenic, fluoride and iodine in groundwater of China (Review). Journal of Geochemical Exploration, 135: 1−21. DOI：10.1016/j. gexplo.2013.10.012.

Xiao J, Zhang F, Jin ZD. 2016. Spatial characteristics and controlling factors of chemical weathering of loess in the dry season in the middle Loess Plateau, China. Hydrological Processes, 30(25): 4855−4869. DOI：10.1002/hyp. 10959.

Xiao Q, Shen LC, Yuan DX, et al. 2011. Using $\delta^{18}O$ and $\delta^{34}S$ isotopic techniques to trace the recycling process of hot springs in Chongqing metropolitan. Journal of Chongqing University, 34(5): 89−94. (in Chinese) DOI：10. 11835/j.issn.1000-582X.2011.05.016.

Xie YX, Tan KO, Zuo ZH. 1981. Report on the hydrogeological survey of the Guang'an amplitude region: Nanjiang Hydrogeological Brigade of Sichuan Geological Bureau. (in Chinese)

Xing SP, Wu P, Hu XD, et al. 2023. Ceochemical characteristics of aquifer sediments and their influence on fluoride enrichment in groundwater in the Hualong-Xunhua Basin. Earth Science Frontiers, 30(2): 526−538. (in Chinese) DOI：10.13745/j.esf.sf.2022.9.10.

Yan ZX, Feng MG. 2022. Hydrochemical characteristics and driving factors of surface water in the mining area of Changhe River Basin. Environmental Chemistry, 41(2): 632−642. (in Chinese) DOI：10.7524/j.issn.0254-6108.

2020101505.

Zhang LQ, Dong DL, Lv S, et al. 2023. Spatial evolution analysis of groundwater chemistry, quality, and fluoride health risk in southern Hebei Plain, China. Environmental Science and Pollution Research, 30(21): 32−51. DOI：10.1007/s11356-023-26316-7.

Zhang MH, Zhou SY, Liu DD, et al. 2024. Characteristics and genesis of groundwater salinization in coastal areas of the Lower Reaches of Oujiang Basin. Journal of Groundwater Science and Engineering, 12(2): 190−204. DOI：10.26599/jgse.2024.9280015.

Zhang W, Hao CM, Lin DJ, et al. 2021. Study on the fluorine distribution and formation of high fluorine middle-level groundwater in Sulin mining area, Anhui. Environmental Pollution and Control, 43(8): 1022−1027. (in Chinese) DOI：10.15985/j.cnki.1001-3865.2021.08.017.

Zhang YT, Wu JH, Xu B. 2018. Human health risk assessment of groundwater nitrogen pollution in Jinghui canal irrigation area of the loess region, northwest China. Environmental Earth Sciences, 77(7): 1. DOI：10.1007/s12665-018-7456-9.

Zhang ZX, Xu M, Zhang Q, et al. 2018. Hydrogeochemistry, genesis and water quality analysis of shallow groundwater in red-bed area of the Mianyang city. Science Technology and Engineering, 18(3): 168−173. (in Chinese)

Zhao X, Duan X, Wang B, et al. 2016. Environmental exposure related activity patterns survey of Chinese population (Children). China: Beijing: China Environmental Science Press. (in Chinese)

Zhou YZ, Zeng YY, Zhou JL, et al. 2016. Distribution of groundwater arsenic in Xinjiang, P. R. China. Applied Geochemistry, 77(2): 116−125. DOI：10.1016/j.apgeochem.2016.09.005.

Zhu YP, Su CL, Liang C, et al. 2015. Effects of sediment lithology and groundwater hydrochemical characteristics on fluorine transport at water soil interface. Geological Science and Technology Information, 34(5): 160−165. (in Chinese)